

# The magnetization process of classical Heisenberg magnets with non-coplanar cuboc ground states

Johannes Richter,<sup>1</sup> Heinz-Jürgen Schmidt,<sup>2,\*</sup> and Jürgen Schnack<sup>3</sup>

<sup>1</sup>*Institut für Physik, Universität Magdeburg, P.O. Box 4120, D-39016 Magdeburg, Germany*

<sup>2</sup>*Fachbereich Mathematik, Informatik, Physik, Universität Osnabrück, 49069 Osnabrück, Germany.*

<sup>3</sup>*Fakultät für Physik, Universität Bielefeld, P.O. Box 100131, 33501 Bielefeld, Germany.*

(Dated: April 26, 2024)

We consider a classical Heisenberg model on the kagomé and the square kagomé lattice, where at zero magnetic field non-coplanar cuboctahedral ground states with twelve sublattices exist if suitable exchange couplings are introduced between the other neighbors. Such 'cuboc ground states' are remarkable because they allow for chiral ordering. For these models, we discuss the magnetization process in an applied magnetic field  $H$  by both numerical and analytical methods. We find some universal properties that are present in all models. The magnetization curve  $M(H)$  usually contains only non-linear components and there is at least one magnetic field driven phase transition. Details of the  $M(H)$  curve such as the number and characteristics (continuous or discontinuous) of the phase transitions depend on the lattice and the details of the exchange between the further neighbors. Typical features of these magnetization processes can already be derived for a paradigmatic 12 spin model that we define in this work.

PACS numbers: 75.10.Jm, 75.50.Xx, 75.40.Mg

## I. INTRODUCTION

Heisenberg antiferromagnets on two-dimensional lattices of corner-sharing triangles are the prototypes of highly frustrated magnets. The celebrated kagomé antiferromagnet (KHAF) is the most prominent example. Already in the classical limit the model exhibits unconventional properties. The corner-sharing triangular geometry leads to a highly degenerate ground-state manifold including coplanar as well as non-coplanar spin configurations [1–4]. Quantum fluctuations select the coplanar  $\sqrt{3} \times \sqrt{3}$  state [5–8]. The investigation of the low-temperature physics of the classical model is also highly non-trivial since the free energy exhibits many different local minima with entropic barriers between them [9, 10].

Another spin system on a lattice with corner-sharing triangles is the square-kagomé Heisenberg antiferromagnet (SKHAF). The model was introduced about 20 years ago [11–21]. Over the last 5 years the SKHAF has attracted more and more attention on the theoretical [22–31] and experimental [32–36] side. The SKHAF shares many properties with the KHAF, such as a highly degenerate ground-state manifold including coplanar  $\sqrt{3} \times \sqrt{3}$  and  $q = 0$  states [15, 27, 30], the absence of magnetic order in the quantum  $s = 1/2$  model [15–17, 24, 27, 28], and flat-band phenomena emerging in applied magnetic field [21, 37]. Moreover, the SKHAF and the KHAF exhibit similar thermodynamic properties for the quantum  $s = 1/2$  [38–41] as well as for the classical model [9, 10, 30].

For both models the massive degeneracy of the classical ground-state manifold can be lifted by additional ex-

change couplings such as 2nd-nearest neighbor and 3rd-nearest neighbor bonds, see, e. g., [30, 42–46]. However, to find the classical ground state for such models sometimes appears to be challenging, in particular if the Luttinger-Tisza method fails, see e.g. [30, 46, 47].

Of particular interest is the quest for classical Heisenberg models with exclusively non-coplanar ground states. In this case finite-temperature phase transitions in two-dimensional Heisenberg models can emerge, which do not contradict the famous Mermin-Wagner theorem [48]. Prominent examples of non-coplanar classical ground states on two-dimensional lattices are the so-called cuboc1, cuboc2 and cuboc3 phases. These phases exhibit 12 non-coplanar sublattices pointing towards the 12 vertices of the cuboctahedron. Such classical non-coplanar ground states are candidates as parents for chiral spin liquids in corresponding quantum spin models [42, 49, 50].

The cuboc2 phase was found in Ref. [42] for the classical KHAF with ferromagnetic nearest-neighbor exchange  $J_1$  and antiferromagnetic 2nd neighbor exchange  $J_2$ . The cuboc1 phase was first reported in Refs. [43, 51] for the classical KHAF with antiferromagnetic nearest-neighbor exchange  $J_1$  and 3rd neighbor exchange  $J_d$  along the diagonals of the hexagons. Later on, in Ref. [44] a systematic analysis of these phases was given and the notations cuboc1 and cuboc2 were introduced. All neighbouring pairs of spins form an angle of  $120^\circ$  (cuboc1) or  $60^\circ$  (cuboc2).

Very recently, cuboc phases were found and analyzed also for the classical SKHAF with further-neighbor exchange  $J_+$  and  $J_x$  along the diagonals of the octagons of the square-kagomé lattice [30]. For this model, except the cuboc1 phase already known from the KHAF, a new cuboc3 phase was detected, featuring two different angles between neighbouring spin pairs,  $120^\circ$  and  $60^\circ$ , associated with the two non-equivalent nearest-neighbor

\* [hschmidt@uos.de](mailto:hschmidt@uos.de)

bonds of the SKHAF.

In the present paper we focus on the ground-state magnetization process of classical Heisenberg models having cuboc ground states in zero magnetic field. The corresponding Hamiltonian augmented with a Zeeman term is given by

$$\mathcal{H} = \sum_{i < j} J_{ij} \vec{s}_i \cdot \vec{s}_j - H \sum_i s_i^z, \quad |\vec{s}_i| = 1. \quad (1)$$

For most classical Heisenberg antiferromagnets the ground-state magnetization  $M = \sum_i s_i^z$  increases linearly up to saturation  $M_{\text{sat}} = N$ , where  $N$  is the number of spins. Thus, for the KHAF and the SKHAF with only nearest-neighbor bonds  $J_1$  the magnetization is given by  $M/N = H/(6J_1)$ ,  $H \leq H_{\text{sat}} = 6J_1$ , see, e.g., Ref. [52]. On the contrary, the magnetization curves of the quantum KHAF and SKHAF exhibit plateaus and jumps [15, 16, 53–55]. In general, the linearity of the classical magnetization curve may have different reasons. In the case of the KHAF and the SKHAF with only nearest-neighbor bonds it follows from the existence of coplanar ground states with vanishing total spin for  $H = 0$ . As the magnetic field increases, the spin vectors are folded in the direction of the magnetic field axis, much like the ribs of a closing umbrella. The resulting 3-dimensional configuration is therefore also called the “umbrella construction”. In the cases of the KHAF and the SKHAF with additional bonds and non-coplanar zero-field cuboc ground states the above-sketched umbrella construction is no longer possible. Interesting enough, there exists an analogous, purely mathematical 4-dimensional umbrella construction, but this yields non-physical ground states [56]. It is thus plausible that the search for physical, i. e., at most 3-dimensional ground states leads to different phases and nonlinear magnetization curves.

Over the last two decades, for the isotropic Heisenberg antiferromagnet only a few examples of classical magnetization curves with jumps were reported for finite systems with icosahedral symmetry or fullerene molecules [57–63]. However, quite recently in Refs. [64] and [65] unconventional classical magnetization curves with jumps and kinks have been found for a frustrated spinel, the  $J_1$ - $J_d$  KHAF as well as for the SKHAF with further-neighbor bonds. Significantly, in these cases there is always a 3-dimensional ground state for  $H = 0$  with vanishing total spin, which, according to the above, makes sense.

In this study we discuss all classical spin lattices known to us in which a cuboctahedral ground state is reported in the literature and compare their magnetization curves. In particular, we consider four two-dimensional classical spin-lattice models: the kagomé  $J_1$ - $J_2$  magnet with  $J_1 < 0$ ,  $J_2 > 0$ , the kagomé  $J_1$ - $J_d$  magnet with  $J_1, J_d > 0$  and the square-kagomé  $J_1$ - $J_+$ - $J_x$  magnet with  $J_1, J_+ = J_x > 0$  and with  $J_1 < 0$  and  $J_+ = J_x > 0$ . Note that in all these cases the lack of coplanar classical ground states, i. e., the existence of only non-coplanar ground states, is related to additional further-neighbor bonds. The focus is here on the kagomé models since for the kagomé  $J_1$ - $J_2$

magnet so far no analysis of the classical magnetization curve is available. We also briefly consider the kagomé  $J_1$ - $J_d$  magnet with  $J_1, J_d > 0$  and the square-kagomé  $J_1$ - $J_+$ - $J_x$  for comparison and add some new data not presented in Refs. [64] and [65]. Before we deal with these lattice models, we consider as an introductory and characteristic example a classical Heisenberg model for a spin system with 12 spins, in which the ground state is unique with a suitable arrangement of three different exchange bonds and becomes a non-coplanar cuboc state.

For this finite system of  $N = 12$  spins we will provide several analytical expressions for the magnetization curve. We will also demonstrate that many features of the magnetization of the kagomé and square-kagomé spin lattices are already present in the simpler 12 spin model. In addition, the small number of only  $N = 12$  spins allows quantum mechanical calculations for spin quantum numbers up to  $s = 9/2$ , which we use for comparison with the classical results.

## II. METHODS

Let us briefly describe the used methods. We use a variant of the iterative minimization method to get numerical ground-state data for the spin configuration, the energy  $E_0$  and the magnetization  $M$ . This method is described in more detail in Ref. [65].

We also use a semi-analytical approach introduced in [30, 65], which we will describe here briefly for convenience. We use numerical data as input to figure out groups of spins approximately pointing into the same direction. Based on the lattice symmetries we determine the symmetry group of the resulting spin orientations, which eventually allows to reduce the number of different spin orientations. The energy  $E$  is then written as a function of a few parameters  $\alpha_i$ , i. e.,  $E = \mathcal{H}(\alpha_1, \dots, \alpha_n)$ , and can be minimized analytically or numerically. The criterion for the success of the semi-analytical method is the lowering of the resulting ground state energy compared to the corresponding numerical value. This method enables the exact calculation of the boundaries between individual ground state phases, and thus the construction of precise phase diagrams.

In special cases, typically for the last phase before saturation, the number of free parameters for the ground states is so small that an analytical calculation becomes possible. Alternatively, a generalized Luttinger-Tisza method can be used for this purpose [47]. To illustrate our approach, in the next section we present both the semi-analytical and the fully analytical solution for the 12 spin model in detail.

We often use so-called “common origin plots” to visualize classical ground states. In a common origin plot, the spin vectors of a ground state, which belong to the different spin sites, are plotted in a single unit sphere. Although this means that the exact information about the distribution of the spin vectors on the lattice is lost,

structures and symmetries that characterize the ground state in more detail often become visible.

### III. THE 12 SPIN MODEL

The cuboctahedron is one of the 13 Archimedean solids and is created by joining the centers of the 12 edges of the cube. The set of rotations and reflections leaving the cuboctahedron invariant generates a 'natural' 12-dimensional linear representation of the octahedral group  $\mathcal{O}_h$  of order 48.

The Heisenberg model on the cuboctahedron was studied for the quantum [66, 67] as well as for the classical model [68]. In case of only nearest-neighbor exchange  $J_1$  the classical ground-state manifold contains coplanar as well as non-coplanar states and the magnetization curve is a simple straight line.

For our purposes, we consider the inverse problem, namely how to define suitable exchange bonds between  $N = 12$  spin sites so that the resulting ground state forms a cuboctahedron in *spin space*. Obviously,  $N = 12$  is the lowest number of spins with a cuboc ground state. The details of the solution can be found in the Appendix. As the result, we obtain the '12 spin model', i. e., an exchange matrix  $\{J_{ij}\}$  with three different exchange bonds  $J_1 = -1$ ,  $J_2 = 1$ ,  $J_3 = 2$ . It commutes with the natural 12-dimensional representation of  $\mathcal{O}_h$ , i. e., it has full  $\mathcal{O}_h$  symmetry. A graphical representation is given in the left panel of Fig. 1. It is also possible to arrange the 12 spins on the vertices of the cuboctahedron as it is shown in the right panel of Fig. 1. Note, however, that the above choice of exchange bonds  $J_1$ ,  $J_2$ ,  $J_3$  and the corresponding arrangement of spins on the cuboctahedron is not unique. An interchange of  $J_1$  and  $J_2$ , i. e., a parameter set  $J_1 = 1$ ,  $J_2 = -1$ ,  $J_3 = 2$  and a corresponding arrangement of spins on the cuboctahedron is equivalent. As a result, the assignment of the cuboc ground state to either the cuboc1 or cuboc2 states found for lattice models is not reasonable, since it depends on the arrangement of the bonds.

In what follows we present the main findings for the magnetization process of the 12 spin model. The magnetization process is shown in Fig. 2. The most striking feature of the magnetization curve is a continuous phase transition at  $H_c = 2(3 - \sqrt{3}) \approx 2.5359$  characterized by a significant kink in  $M(H)$  at  $H_c$ . Moreover, the magnetization curve  $M(H)$  is nonlinear and the ground state is non-coplanar in the whole region  $0 \leq H < H_{\text{sat}} = 8$ . The magnetization at the transition is  $M(H_c) = M_{\text{sat}}/3$ .

For the low-field phase at  $H < H_c$  we use our semi-analytical approach. The ground state is a deformed cuboc state which consists of three groups of spins forming squares with respective polar angles  $\theta_i$ ,  $i = 1, 2, 3$ .

Its energy is given by

$$E(\theta_1, \theta_2, \theta_3; H) = \frac{1}{3} \left\{ \cos(\theta_1) [4 \cos(\theta_2) - H] - H \cos(\theta_2) - H \cos(\theta_3) - \sin^2(\theta_3) - 2 \sin(\theta_1) \sin(\theta_2) - 2\sqrt{2} [\sin(\theta_1) \sin(\theta_3) + \sin(\theta_2) \sin(\theta_3)] - \cos^2(\theta_1) - \cos^2(\theta_2) + \cos^2(\theta_3) \right\}. \quad (2)$$

The polar angles are found numerically by searching for the minimum of  $E(\theta_1, \theta_2, \theta_3; H)$  for fixed  $H$ . We show the deformed cuboc ground state in Fig. 3, left panel, where the three groups of spins are presented as red, blue and green arrows pointing to three squares, where the green square is twisted by  $45^\circ$ . The respective  $z$ -components as a function of the field  $H$  are shown in Fig. 4. Interestingly, the  $z$ -component  $s_{\text{red}}^z$  of the red group of spins shows a non-monotonic behavior. After the expected increase of  $s_{\text{red}}^z$  at low fields it rapidly drops down as  $H \rightarrow H_c$ , even with an infinite slope at  $H = H_c$ . We notice that also the  $z$ -component of the blue group of spins exhibits an infinite slope as approaching the transition from below. On the other hand, the slope of the magnetization at  $H = H_c$  remains finite:  $\lim_{H \uparrow H_c} \frac{\partial M}{\partial H} = \frac{1}{47} (21 + 10\sqrt{3}) \approx 0.81533$ .

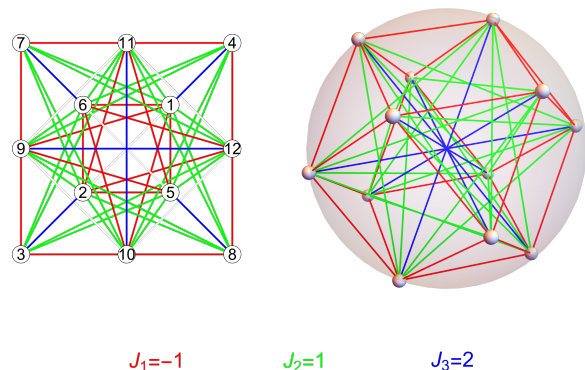


Figure 1. Exchange matrix  $\{J_{ij}\}$  leading to the cuboc state of the 12 spin model, planar and three-dimensional representation.

For the phase at  $H > H_c$  we can present a full analytical description. The ground state consists now of two groups of spins forming squares with respective polar angles  $\theta_i$ ,  $i = 1, 2$ . The energy of this state is given by

$$E(\theta_1, \theta_2; H) = \frac{1}{6} H [2 \cos(\theta_1) + \cos(\theta_2)] + \frac{1}{6} [-8\sqrt{2} \sin(\theta_1) \sin(\theta_2) + 4 \cos(2\theta_1) + 2 \cos(2\theta_2)]. \quad (3)$$

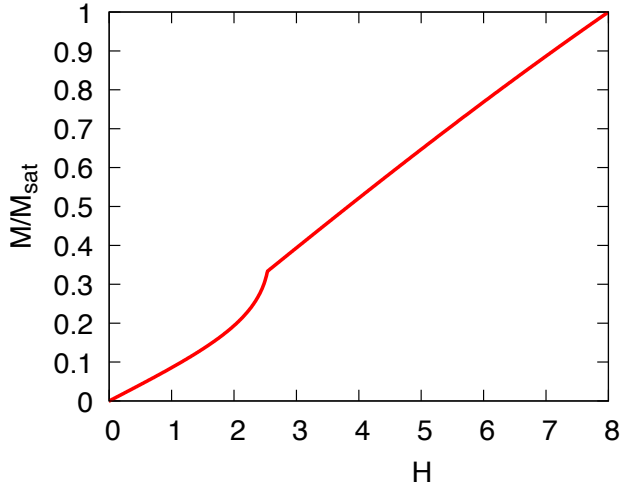


Figure 2. Magnetization process of the  $J_1$ - $J_2$ - $J_3$  12 spin model with a cuboc ground state. We observe a kink at  $H = H_c = 2.5359$  and  $M = M_c = \frac{1}{3}M_{\text{sat}}$ .

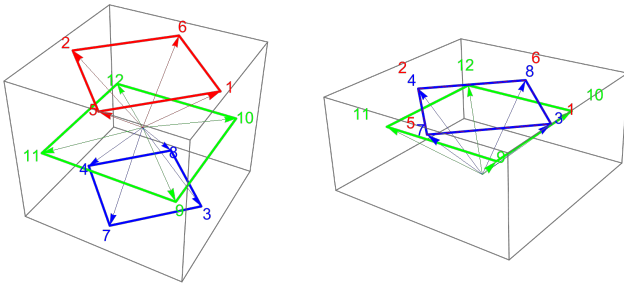


Figure 3. Representation of the ground states of the 12 spin model at low and high magnetic fields; left  $H = 1.5 < H_c$ , right  $H = 5 > H_c$ .

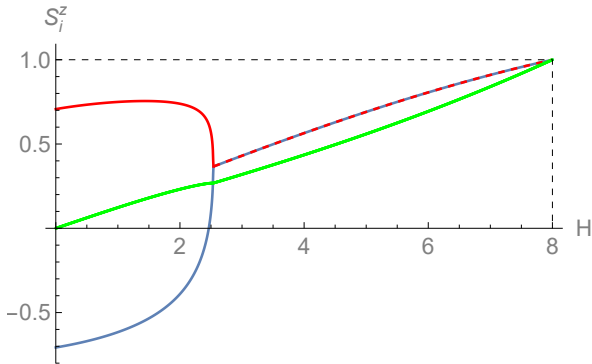


Figure 4. The  $z$ -components of the spin vectors of the 12 spin model in dependence on the magnetic field. The colors of the lines correspond to the colors used for the arrows in Fig. 3.

The ground state satisfies  $\frac{\partial E}{\partial \theta_1} = \frac{\partial E}{\partial \theta_2} = 0$  which can be solved for a parametric representation in terms of  $z \equiv$

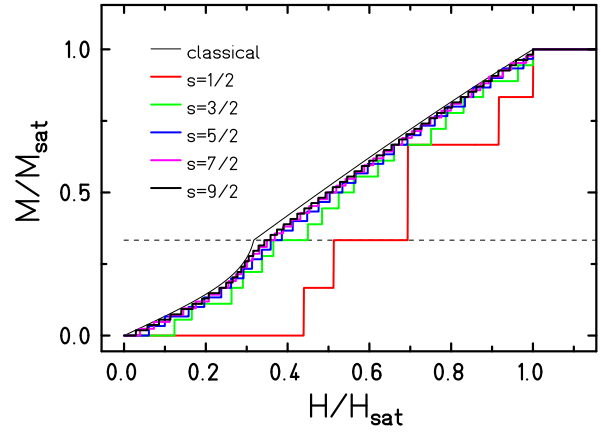


Figure 5. Magnetization curves for the quantum 12 spin model and various spin quantum numbers  $s = \frac{1}{2}, \dots, \frac{9}{2}$ .

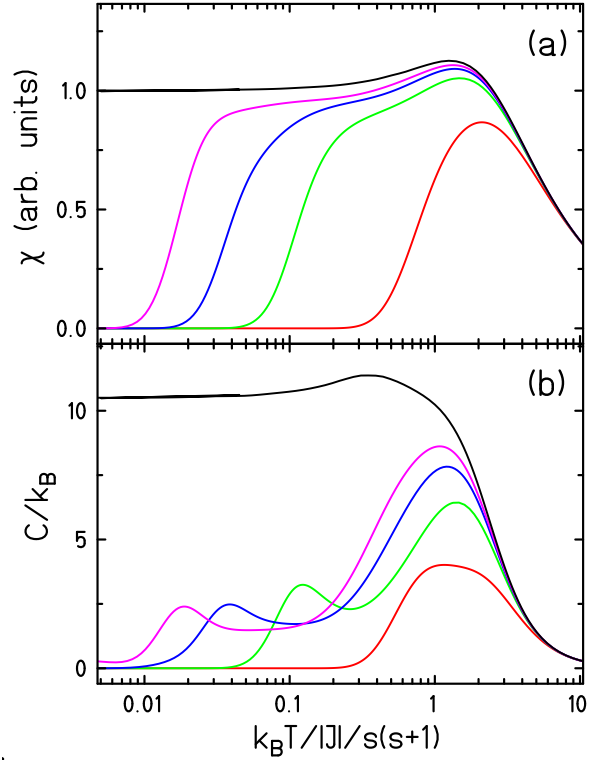


Figure 6. Susceptibility  $\chi$  and specific heat  $C$  for the quantum 12 spin model and various spin quantum numbers  $s = \frac{1}{2}, \dots, \frac{7}{2}$  as function of the scaled temperature  $\frac{k_B T}{|J|s(s+1)}$ . The color codes are identical to those in Fig. 5.

$\cos \theta_2$ :

$$\cos \theta_1 = \frac{\sqrt{2}z}{\sqrt{z^2 + 1}}, \quad (4)$$

$$H = 4z \left( \frac{\sqrt{2}}{\sqrt{z^2 + 1}} + 1 \right), \quad (5)$$

$$M = \frac{1}{3} \left( \frac{2\sqrt{2}z}{\sqrt{z^2 + 1}} + z \right). \quad (6)$$

We mention, that these equations, in principle, allow to find an analytical expression for  $M(H)$  by eliminating the parameter  $z$ , however, in form of the cumbersome expressions of the roots of a 4th order polynomial. The spin configuration is a 'double umbrella' state, see Fig. 3, right panel, where the two groups of spins are presented as blue and green arrows pointing to two squares twisted by  $45^\circ$ . The blue group is the merging of the former blue and red groups of spins of the low-field phase, i.e., it contains 8 spins. As the magnetic field approaches the saturation field, both umbrellas converge toward the north pole. If the magnetic field approaches  $H_c$  from above we have  $\lim_{H \downarrow H_c} \frac{\partial M}{\partial H} = (15 + 2\sqrt{3})/142 \approx 0.130029$ . This yields a jump of the susceptibility of  $\Delta\chi \approx -0.685301$  at  $H = H_c$ .

Finally, we consider the quantum-mechanical 12 spin model. With the exchange interactions given in Fig. 1 the ground state, i. e.,  $T = 0$  magnetization curve of the quantum spin model can numerically be obtained for spin quantum numbers up to  $s = 9/2$  using a Lanczos procedure [69]. Figure 5 shows the respective magnetization curves for half-integer spin quantum numbers. Apart from the case  $s = 1/2$  the quantum curves approach the classical curve closely from below, and the larger  $s$  is, the more so. For the largest available spin of  $s = 9/2$ , even the non-linear increase into the kink is clearly visible.

For completeness, we also show the temperature dependence of the magnetic susceptibility as well as of the heat capacity for 12 spin model systems with single-spin quantum number of up to  $s = 7/2$ , see Fig. 6. For small spin quantum numbers exact diagonalization was used, otherwise the thermal quantities were calculated using the finite-temperature Lanczos method [70]. For the interested reader we like to point out that the susceptibility approaches the classical limit much quicker with increasing  $s$  than the heat capacity.

In the following sections we consider lattice models. We will see that features observed for the 12 spin model are also present for extended systems. Thus this model may serve as a paradigm for a classical magnetization curve starting from a cuboc ground ground, which allows a comprehensive (semi-)analytical description of the magnetization process.

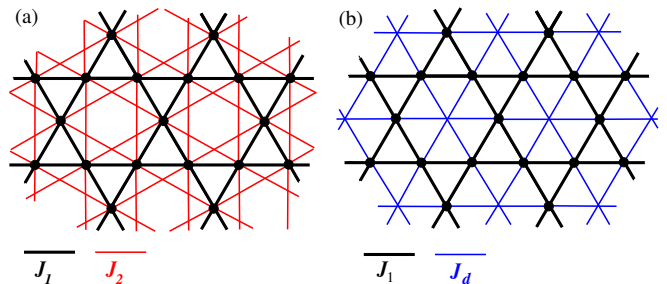


Figure 7. Sketch of the  $J_1$ - $J_2$  (a) and the  $J_1$ - $J_d$  (b) model on the kagomé lattice.

## IV. THE HEISENBERG MODEL ON THE KAGOMÉ LATTICE WITH CUBOC PHASES

### A. The $J_1$ - $J_2$ model

As reported in Refs. [42] and [44] a zero-field cuboc ground state of the type cuboc2 exists for the  $J_1$ - $J_2$  Heisenberg model with ferromagnetic nearest-neighbor bonds  $J_1$  and antiferromagnetic 2nd neighbor bonds  $J_2$  (see Fig. 7 (a)), if  $J_2/|J_1| \geq 1/3$ . We set the energy scale by choosing  $J_1 = -1$ . The saturation field is then given by  $H_{\text{sat}} = 6(J_2 - 1/3)$ . In what follows, we will demonstrate that the general features of the magnetization process of the  $J_1$ - $J_2$  kagomé model are quite similar to those of the 12 spin model. In particular, there are two phases with three groups of spins below a critical field  $H_c$  and with two groups of spins for  $H > H_c$ , the magnetization curve  $M(H)$  is nonlinear and the ground state is noncoplanar in the whole region  $0 \leq H < H_{\text{sat}}$ .

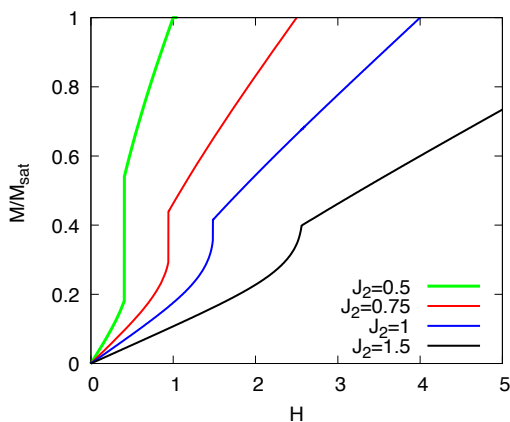


Figure 8. Magnetization curves of the  $J_1$ - $J_2$  Heisenberg model on the kagomé lattice for  $J_1 = -1$  and various values of  $J_2$  (see legend).

Similarly as in Sec. III we can use the semi-analytical approach below  $H_c$ , and we can provide a full analytical description above  $H_c$  in form of a  $J_2$ -dependent parametric representation similar to Eqs. (4) - (6). We show a few magnetization curves in Fig. 8. The spin configurations

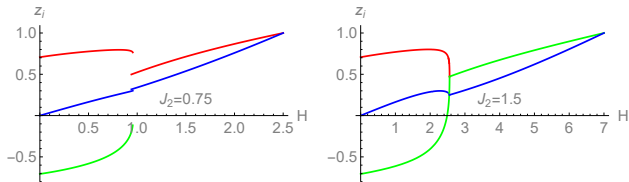


Figure 9. The  $z$ -components of the spin vectors of of the  $J_1$ - $J_2$  Heisenberg model on the kagomé lattice for  $J_1 = -1$  and  $J_2 = 0.75$  (left panel) and  $1.5$  (right panel) in dependence on the magnetic field.

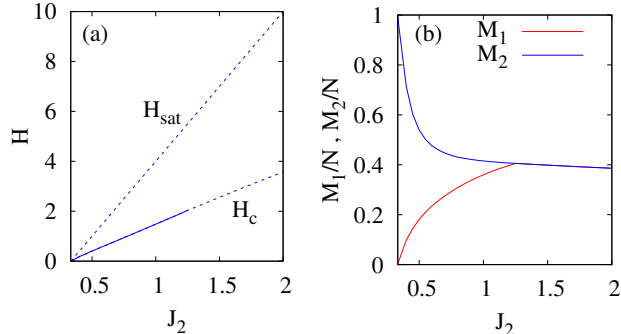


Figure 10. (a) Phase diagram for the  $J_1$ - $J_2$  kagomé model (solid lines - discontinuous transitions, dashed lines - continuous transitions). (b) Magnetizations  $M_1, M_2$  at the critical field  $H_c$  in dependence on  $J_2$  for the  $J_1$ - $J_2$  kagomé model.

of the two phases below and above  $H_c$  are very similar to those shown in Fig. 3, i.e., there is a deformed cuboc state which consists of three groups of spins at low field and a double umbrella state at high fields.

In contrast to the 12 spin model the phase transition at the critical field  $H_c$  is either continuous or discontinuous depending on the magnitude of  $J_2$ . For  $J_2 < J_m \approx 1.25221$  there is a jump at  $H_c$  in the magnetization curve, whereas for  $J_2 \geq J_m$  the  $M(H)$  curve exhibits a kink at  $H_c$ . We mention that for  $J_2 = J_m$  the differential susceptibility diverges as approaching  $H_c$  according to  $dM/dH \sim (H_c - H)^{-1/2}$ . It should be noted, however, that this relationship as well as the previous remarks do not represent rigorous results, but rather were obtained by analyzing numerical data from the semi-analytical approach. In Fig. 8 we notice the jump for  $J_2 = 0.5, 0.75$ , and  $1.0$ , but only a kink for  $J_2 = 1.5$ . In Fig. 9 we show the  $z$ -components of the spin vectors as a function of the field  $H$  for two representative parameter sets  $J_2 = 0.75$  and  $1.5$ . For  $J_2 = 1.5$  the striking analogy to Fig. 4 is obvious. But also for  $J_2 = 0.75$  the same two phases are present, however, with an abrupt change of the spin configuration at the transition point  $H_c$ . Finally we present in Fig. 10 the saturation field  $H_{\text{sat}}$ , the critical field  $H_c$  as well as the magnetizations  $M_1$  and  $M_2$  at  $H_c$  as functions of  $J_2$ .

## B. The $J_1$ - $J_d$ model

According to Refs. [43, 51] and [44] another zero-field cuboc ground state, now of the type cuboc1, exists for the kagomé  $J_1$ - $J_d$  Heisenberg model with antiferromagnetic nearest-neighbor bonds  $J_1$  and antiferromagnetic 3rd neighbor bonds  $J_d$  along the diagonals of the hexagons, see Fig. 7(b). Some results for the magnetization curves of these systems have already been published in Ref. [64], in particular for  $J_d = 0.1 J_1$  and  $J_d = 0.5 J_1$ . We were able to confirm these results, but have to make some restrictions due to finite-size effects for the case  $J_d = 0.1$ , see below.

In what follows we set the energy scale by choosing  $J_1 = 1$ . The saturation field is then given by  $H_{\text{sat}} = 6 + 4 J_d$ . Again we will observe that the magnetization process exhibits similarities to the 12 spin model discussed in Sec. III. The influence of the magnetic field on the ground states of the kagomé lattice is summarized in the phase diagram shown in Fig. 11.

Additional to the ferromagnetic phase FM and the cuboc1 phase for  $H = 0$  we encounter three non-coplanar phases denoted by I, II and III. Phase I and II prevail at low fields and represent two different types of deformed cuboc1 states, each consisting of three groups of spins with constant  $z$ -components. As for the previous models, in the high-field phase III just before saturation a full analytical description is possible in form of a  $J_d$ -dependent parametric representation similar to Eqs. (4) - (6). We omit the explicit form because it is too complicated.

According to the phase diagram there are three kinds of magnetization processes with different transitions between the various phases.

1. For smaller values  $J_d \lesssim 0.341$  there is one discontinuous transition I - III, see the example for  $J_d = 0.25$  in Fig. 12 showing the magnetization curve and the  $z$ -components of the spins in the ground state depending on  $H$ .
2. For intermediate values  $0.341 \lesssim J_d \lesssim 0.694$  there is one discontinuous transition I - II and one continuous one II - III, which are located close to each other. Corresponding data for  $J_d = 0.55$  are shown in Fig. 13.
3. At larger values  $J_d \gtrsim 0.694$  there is only one continuous transition II - III, see Fig. 14, and the overall behavior of the magnetization and the  $z$ -components corresponds to that of the 12 spin model.

For a certain region with  $J_d \lesssim 0.45$  our numerical data are not entirely conclusive since the phase transitions depend on the number  $N$  of spins considered in the model, see Figure 15. These finite-size effects are possibly due to tiny energy differences between the phases that occur at small values of  $J_d$ .

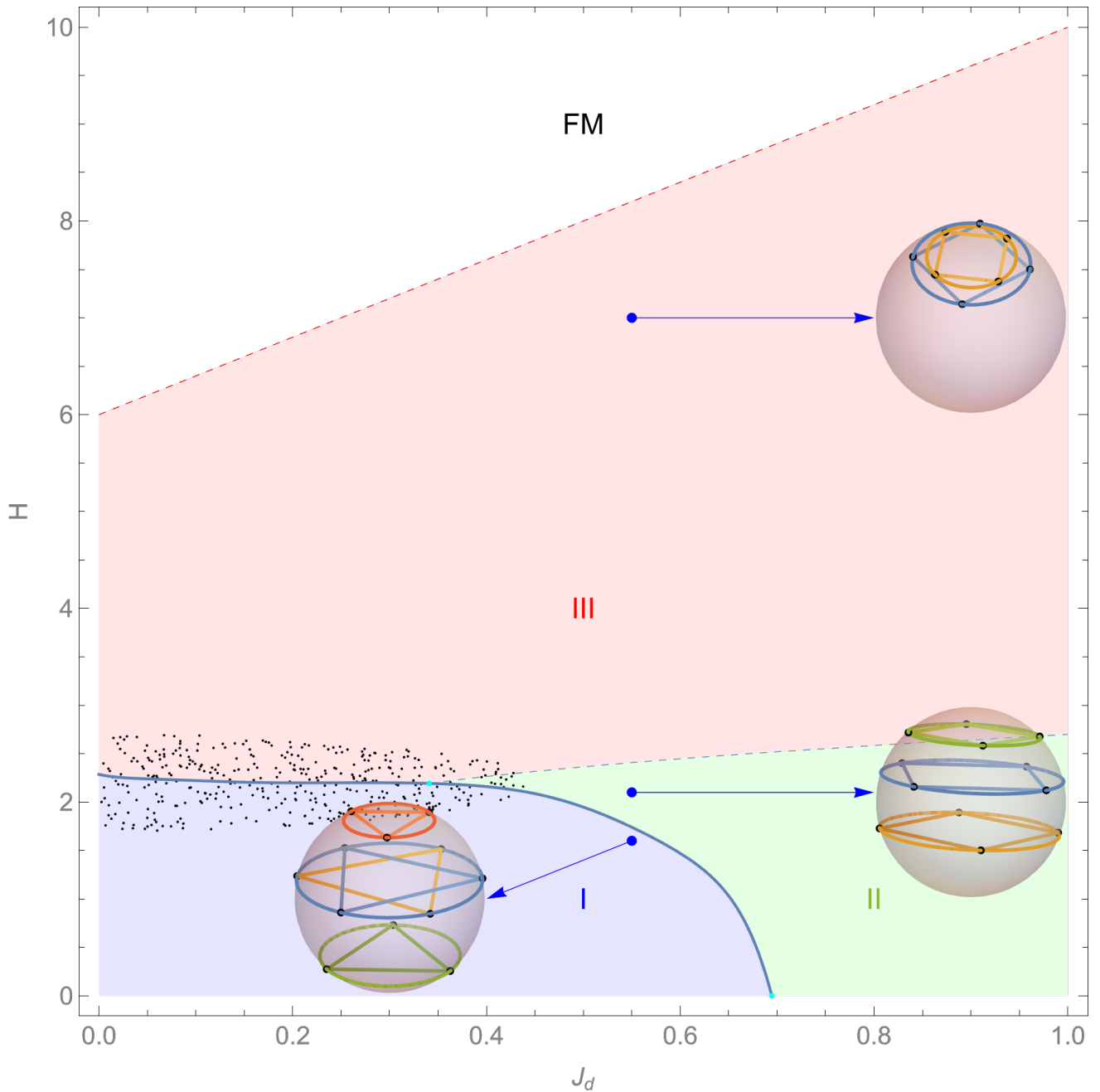


Figure 11. Phase diagram of the  $J_1$ - $J_d$  kagomé model setting  $J_1 = 1$ . The horizontal axis represents  $0 \leq J_d \leq 1$  and the vertical axis the magnetic field  $0 \leq H \leq 10$ . We observe three phases denoted by I, II and III with typical common origin plots inserted. Solid curves indicate discontinuous phase transitions and dashed curves continuous ones. In the dotted region, the phases and their boundaries are uncertain due to finite-size effects.

## V. THE HEISENBERG MODEL ON THE SQUARE-KAGOMÉ LATTICE WITH CUBOC PHASES

The magnetization process as well as the relevant theoretical approaches for the Heisenberg model on the square-kagomé lattice with cuboc phase have been discussed in detail very recently in Ref. [65]. However, in order to obtain a comprehensive picture of the magne-

tization processes of classical Heisenberg systems with zero-field cuboctahedral ground state, it seems useful to recapitulate the main features of the magnetization process for square-kagomé models and to compare them with the models discussed in the previous sections.

A striking contrast to the kagomé model is the existence of two non-equivalent sites A (forming the squares) and B (sitting at the center of the bow ties connecting the squares) as well as two non-equivalent nearest-neighbor

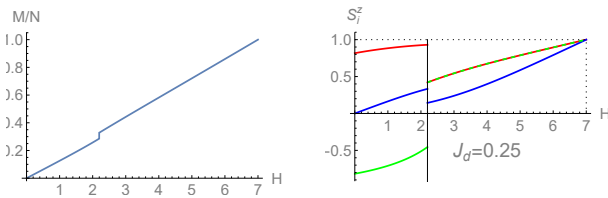


Figure 12. Magnetization curve of the  $J_1$ - $J_d$  Heisenberg model on the kagomé lattice for  $J_1 = 1$  and  $J_d = 0.25$  (left) and corresponding  $z$ -components of the spin vectors (right).

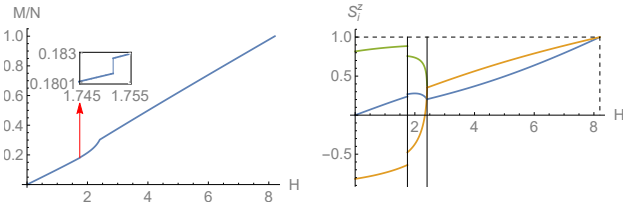


Figure 13. Magnetization curve (left) and corresponding  $z$ -components of the spin vectors (right) of the  $J_1$ - $J_d$  Heisenberg model on the kagomé lattice for  $J_1 = 1$  and  $J_d = 0.55$ . The inset enlarges the scale in order to show the discontinuous phase transition at  $H_c = 1.7515$ .

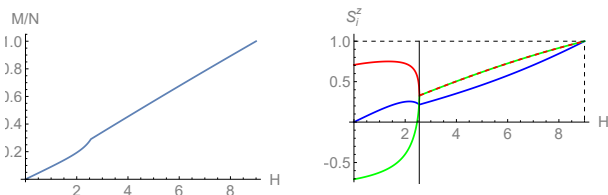


Figure 14. Magnetization curve (left) and corresponding  $z$ -components of the spin vectors (right) of the  $J_1$ - $J_d$  Heisenberg model on the kagomé lattice for  $J_1 = 1$  and  $J_d = 0.75$ .

bonds  $J_1$  and  $J_2$ . A comprehensive study of the zero-field ground-state phase diagram of the classical square-kagomé spin model including cross-plaquette interactions has been presented recently in Ref. [30]. The corresponding model is depicted in Fig. 16.

There are two non-equivalent cross-plaquette interactions  $J_+$  and  $J_x$ . However, the zero-field cuboc ground-state phase is present in the entire parameter region  $J_+, J_x > 0$  independent of the magnitudes of  $J_+$  and  $J_x$ , see Fig. 5 in Ref. [30]. For the sake of simplicity, therefore we consider the symmetric case  $J_+ = J_x =: J_3$ , only.

### A. The model with antiferromagnetic (AF) nearest-neighbor bonds

First we consider the square-kagomé model with  $J_1 = J_2 = 1$  and  $J_3 > 0$ . From Ref. [30] we know that the zero-field ground state is a so-called cuboc1 state, where

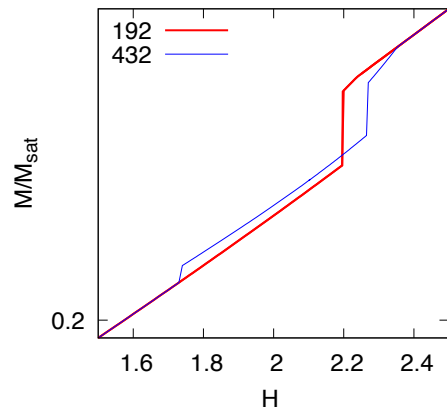


Figure 15. Magnetization curve of the  $J_1$ - $J_d$  Heisenberg model on the kagomé lattice for  $J_1 = 1$  and  $J_d = 0.25$  and the interval  $1.5 < H < 2.5$ . The number of spins  $N = 3L^3$  is chosen as  $N = 192$  and  $N = 432$ . This illustrates the occurrence of finite-size effects in a certain region for  $J_d \lesssim 0.45$ .

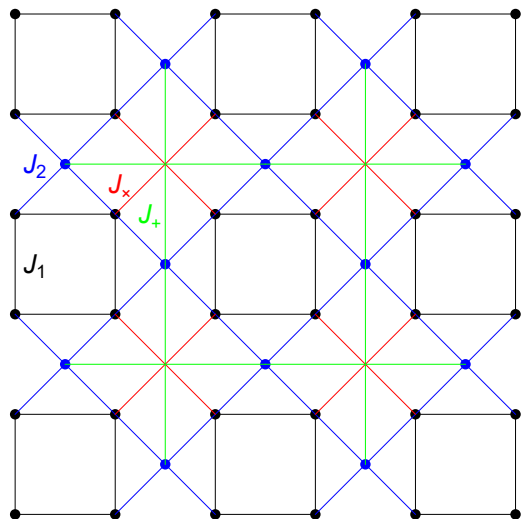


Figure 16. The square-kagomé  $J_1$ - $J_2$  model with cross-plaquette interactions  $J_+$  and  $J_x$ . For the sake of simplicity, we set  $J_+ = J_x = J_3$ . The sites A (black dots) form the squares and the sites B (blue dots) sit in the middle of the bow-ties connecting the squares.

all neighboring pairs of spins form angles of  $120^\circ$ . The saturation field is given by

$$H_{\text{sat}} = 4 + 3J_3 + \sqrt{J_3^2 + 4}. \quad (7)$$

This model shows a rich variety of seven non-coplanar phases as a function of  $J_3$  and  $H$ , denoted by I to VII, see Figure 17. Of the six possible types of magnetization curves, we will only describe the case with small  $J_3$  (e.g. for  $J_3 = 0.1$ ). Here we see three jumps and two kinks corresponding to the phase transitions  $\text{I} \xrightarrow{\mathcal{J}} \text{V} \xrightarrow{\mathcal{J}} \text{VI} \xrightarrow{\mathcal{J}} \text{VII} \xrightarrow{\mathcal{K}} \text{IV} \xrightarrow{\mathcal{K}} \text{FM}$ , see Fig. 18. For more magnetization curves see [30].

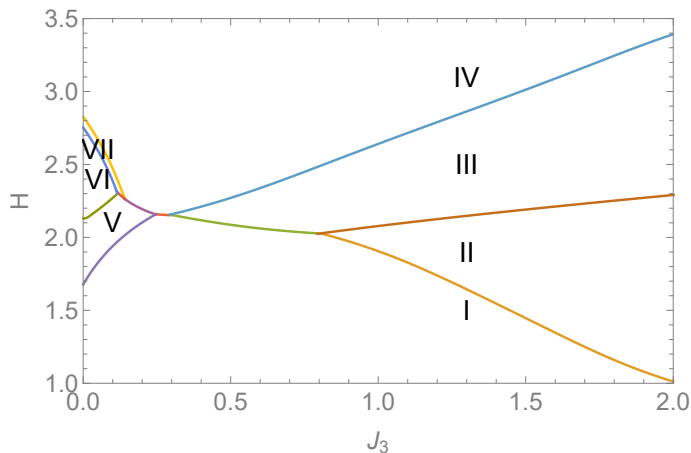


Figure 17. Phase diagram for  $J_1 = J_2 = 1$ . The ferromagnetic phase for  $H \geq H_{\text{sat}}$  is not shown.

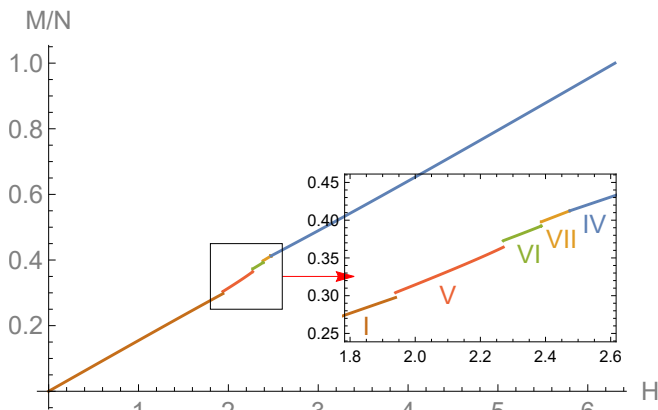


Figure 18. Magnetization curve of the square-kagomé for  $J_1 = J_2 = 1$ ,  $J_3 = 0.1$ . The inset enlarges the scale to make the phase transitions more clearly visible.

The phase I, which passes into the cuboc1 phase for small  $H$ , shows 14 spins (sublattices) in the common origin plot, which are distributed over the north- and south pole of the unit sphere and over three squares, each with constant  $z$  components. For  $H \rightarrow 0$  the four spins of the center square merge in pairs so that the remaining 12 spins form the vertices of a cuboctahedron. Phase IV forms the transition to the  $FM$  ground state and can be described analytically as a common-origin plot of two squares, each with constant  $z$  components, which are rotated by the angle  $45^\circ$  with respect to each other. Also noteworthy is the disordered phase VII, which exists in a narrow strip for small  $J_3$  values, see Figure 17, and can be considered a candidate for a spin liquid due to its high degeneracy.

## B. The model with ferro- and antiferromagnetic (FM/AF) nearest-neighbor bonds

Now we consider the square-kagomé model with  $J_1 = 1$ ,  $J_2 = -1$  and  $0 \leq J_3 \leq 2$ . From Ref. [30] it is known that the zero-field ground state is a so-called cuboc3 state, where each neighboring pair of spins forms an angle of  $120^\circ$  on the squares and an angle of  $60^\circ$  on the triangles.

The saturation field is given by

$$H_{\text{sat}} = 2(1 + J_3), \quad J_3 \leq 2. \quad (8)$$

There are four phases I to IV, such that I, II and III are non-coplanar and IV is coplanar, see Figure 19. Accordingly, there are two types of magnetization curves, the first one corresponding to the sequence of phase transitions  $I \xrightarrow{\mathcal{J}} II \xrightarrow{\mathcal{K}} III \xrightarrow{\mathcal{K}} IV \xrightarrow{\mathcal{K}} FM$ , for  $J_3 > 1.52$ , see Fig. 20 for the example  $J_3 = 1.95$ . The second type of magnetization curves corresponds to the sequence of phase transitions  $I \xrightarrow{\mathcal{J}} III \xrightarrow{\mathcal{K}} IV \xrightarrow{\mathcal{K}} FM$ , for  $J_3 < 1.52$ .

The four phases of the FM/AF square kagomé show certain differences to the AF case. Phase I again consists of 14 spins, but this time arranged in three squares and a pair, so that for  $H \rightarrow 0$  one square degenerates into a pair. Phase III has the same structure but different energy. Phase II, which squeezes between phase I and phase III for  $J_3 > 1.52$  consists of 7 pairs. At the transition  $III \xrightarrow{\mathcal{K}} IV$ , one rectangle and one pair converge towards the north pole, while the other two rectangles merge into one pair. This constitutes the analytical phase IV with three coplanar spins, all of which converge towards the north pole for  $H \rightarrow H_{\text{sat}}$ .

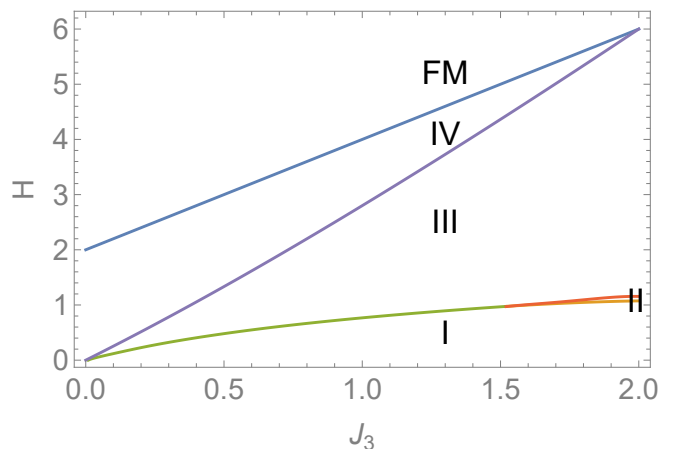


Figure 19. Phase diagram for the FM/AF square kagomé with  $J_1 = -J_2 = 1$ .

## VI. CONCLUSIONS

We have analyzed classical spin-lattice models with cuboctahedral ground states, and compared magnetiza-

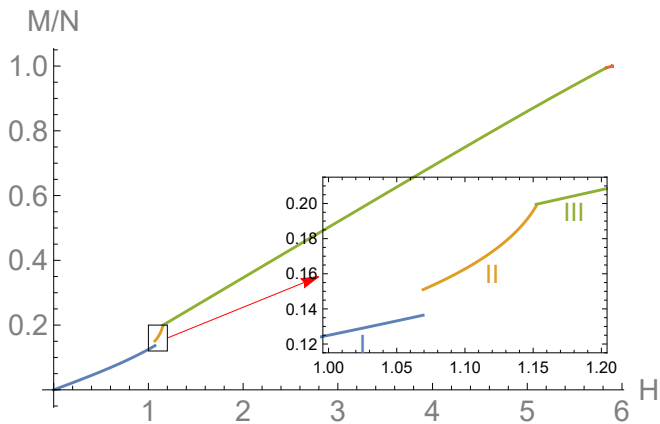


Figure 20. Magnetization curve of the square-kagomé for  $J_1 = -J_2 = 1$ ,  $J_3 = 1.95$ . The inset enlarges the scale to make the phase transitions I  $\rightarrow$  II  $\rightarrow$  III more clearly visible.

tion curves and phase transitions in different systems. The focus here is on the kagomé models, where the classical magnetization curves have not yet been investigated for the  $J_1 - J_2$  variant. In addition, we have compared our findings on the  $J_1 - J_d$  kagomé model with published results and recapitulated our recent study on the  $J_+ = J_\times$  square kagomé lattice. Typical phenomena are different types of deformed cuboc ground states for moderate magnetic fields and, in most cases, double umbrella states approaching the fully aligned state at high fields. Key features of the magnetization process can also be studied using a simplified 12-spin model, which we propose in this work. Interestingly, in the 12-spin model, there are regions of the magnetic field where groups of spins rotate in the opposite direction to the field direction as  $H$  is increased.

The methods used include numerical ground state determination by iterative minimization, a semi-analytical approach and in some cases, especially for the last phase before saturation, fully analytical solutions. These methods allow us to obtain very accurate phase boundaries and phase diagrams.

In summary, our research sheds light on the magnetization process of classical Heisenberg magnets with non-coplanar cuboc ground states and reveal a compli-

cated behavior influenced by the lattice geometry and exchange couplings. This study will hopefully not only improve our understanding of frustrated magnetism, but also contribute to the broader study of exotic magnetic phenomena.

## Appendix A: Construction of the 12 spin model

We recall the problem of defining coupling constants  $J_{i,j}$  between  $N = 12$  spins such that the resulting ground state forms a cuboctahedron in spin space. The vertices  $\mathbf{c}_i$ ,  $i = 1, \dots, 12$  of the cuboctahedron can be chosen as those 12 vectors with exactly one zero component and the other two components being  $\pm 1$ . The normalization factor is irrelevant for the moment. The numbering of the vertices is arbitrary, but for the Fig. 1, left panel, a certain choice of the numbering has been made. We represent these 12 vertices as rows of a  $12 \times 3$  - matrix  $C$  with entries  $C_{ik}$ ,  $i = 1, \dots, 12$ ,  $k = 1, 2, 3$ . Then we define a projector  $P$  in the 12-dimensional space  $\mathbb{R}^{12}$  by

$$P_{ij} = \frac{1}{8} \sum_{k=1}^3 C_{ik} C_{jk}. \quad (\text{A1})$$

It projects onto the 3-dimensional subspace of  $\mathbb{R}^{12}$  spanned by the 3 columns of  $C$ . The symmetric matrix of coupling constants

$$J := 2 \mathbb{1} - 8 P \quad (\text{A2})$$

has zero trace and, moreover, zero diagonal entries. Its non-zero entries are of the form  $J_1 = -1$ ,  $J_2 = 1$ ,  $J_3 = 2$ , as announced in Section III. By construction, the eigenvalues of  $J$  are  $-6$  (3-fold degenerate) and  $2$  (9-fold degenerate). The ground state of the 12 spin model is hence the unique 3-dimensional cuboc state that can be obtained by linear combinations of the eigenvectors corresponding to the lowest eigenvalue  $-6$  of  $J$ .

This method to construct spin systems with given ground states can be generally applied and is not confined to the 12 spin system under consideration.

- 
- [1] J. T. Chalker, P. C. W. Holdsworth, and E. F. Shender, Hidden order in a frustrated system: Properties of the Heisenberg kagomé antiferromagnet, *Phys. Rev. Lett.* **68**, 855 (1992).
  - [2] A. B. Harris, C. Kallin, and A. J. Berlinsky, Possible Néel orderings of the kagomé antiferromagnet, *Phys. Rev. B* **45**, 2899 (1992).
  - [3] D. A. Huse and A. D. Rutenberg, Classical antiferromagnets on the kagomé lattice, *Phys. Rev. B* **45**, 7536 (1992).
  - [4] J. N. Reimers and A. J. Berlinsky, Order by disorder in the classical Heisenberg kagomé antiferromagnet, *Phys. Rev. B* **48**, 9539 (1993).
  - [5] S. Sachdev, Kagome- and triangular-lattice Heisenberg antiferromagnets: Ordering from quantum fluctuations and quantum-disordered ground states with unconfined bosonic spinons, *Phys. Rev. B* **45**, 12377 (1992).
  - [6] A. Chubukov, Order from disorder in a kagomé antiferromagnet, *Phys. Rev. Lett.* **69**, 832 (1992).
  - [7] C. L. Henley and E. P. Chan, Ground state selection in a kagomé antiferromagnet, *J. Magn. Magn. Mater.* **140-144**, 1693 (1995).
  - [8] O. Götze, D. J. J. Farnell, R. F. Bishop, P. H. Y. Li, and

- J. Richter, Heisenberg antiferromagnet on the kagome lattice with arbitrary spin: A higher-order coupled cluster treatment, *Phys. Rev. B* **84**, 224428 (2011).
- [9] M. E. Zhitomirsky, Octupolar ordering of classical kagome antiferromagnets in two and three dimensions, *Phys. Rev. B* **78**, 094423 (2008).
- [10] G.-W. Chern and R. Moessner, Dipolar order by disorder in the classical Heisenberg antiferromagnet on the kagome lattice, *Phys. Rev. Lett.* **110**, 077201 (2013).
- [11] R. Siddharthan and A. Georges, Square kagome quantum antiferromagnet and the eight-vertex model, *Phys. Rev. B* **65**, 014417 (2001).
- [12] J. Schnack, H.-J. Schmidt, J. Richter, and J. Schulenburg, Independent magnon states on magnetic polytopes, *Eur. Phys. J. B* **24**, 475 (2001).
- [13] P. Tomczak and J. Richter, Specific heat of the spin-1/2 Heisenberg antiferromagnet on squagome lattice, *J. Phys. A: Math. Gen.* **36**, 5399 (2003).
- [14] J. Richter, O. Derzhko, and J. Schulenburg, Magnetic-field induced spin-Peierls instability in strongly frustrated quantum spin lattices, *Phys. Rev. Lett.* **93**, 107206 (2004).
- [15] J. Richter, J. Schulenburg, P. Tomczak, and D. Schmalfuß, The Heisenberg antiferromagnet on the square-kagome lattice, *Cond. Matter Phys.* **12**, 507 (2009).
- [16] H. Nakano and T. Sakai, The two-dimensional  $s = 1/2$  Heisenberg antiferromagnet on the shuriken lattice – a lattice composed of vertex-sharing triangles, *J. Phys. Soc. Jpn.* **82**, 083709 (2013).
- [17] I. Rousochatzakis, R. Moessner, and J. v. d. Brink, Frustrated magnetism and resonating valence bond physics in two-dimensional kagome-like magnets, *Phys. Rev. B* **88**, 195109 (2013).
- [18] O. Derzhko, J. Richter, O. Krupnitska, and T. Krokhamlskii, The square-kagome quantum Heisenberg antiferromagnet at high magnetic fields: The localized-magnon paradigm and beyond, *Low Temp. Phys.* **40**, 513 (2014).
- [19] A. Ralko and I. Rousochatzakis, Resonating-valence-bond physics is not always governed by the shortest tunneling loops, *Phys. Rev. Lett.* **115**, 167202 (2015).
- [20] H. Nakano, Y. Hasegawa, and T. Sakai, Magnetization jump in the magnetization process of the spin-1/2 Heisenberg antiferromagnet on a distorted square-kagome lattice, *J. Phys. Soc. Jpn.* **84**, 114703 (2015).
- [21] O. Derzhko, J. Richter, and M. Maksymenko, Strongly correlated flat-band systems: The route from Heisenberg spins to Hubbard electrons, *Int. J. Mod. Phys. B* **29**, 1530007 (2015).
- [22] Y. Hasegawa, H. Nakano, and T. Sakai, Metamagnetic jump in the spin- $\frac{1}{2}$  antiferromagnetic Heisenberg model on the square kagome lattice, *Phys. Rev. B* **98**, 014404 (2018).
- [23] K. Morita and T. Tohyama, Magnetic phase diagrams and magnetization plateaus of the spin-1/2 antiferromagnetic Heisenberg model on a square-kagome lattice with three nonequivalent exchange interactions, *J. Phys. Soc. Jpn.* **87**, 043704 (2018).
- [24] T. Luga, L. D. C. Jaubert, and A. Ralko, Topological nematic spin liquid on the square kagome lattice, *Phys. Rev. Research* **1**, 033147 (2019).
- [25] P. A. McClarty, M. Haque, A. Sen, and J. Richter, Disorder-free localization and many-body quantum scars from magnetic frustration, *Phys. Rev. B* **102**, 224303 (2020).
- [26] Y. Kuno, T. Mizoguchi, and Y. Hatsugai, Flat band quantum scar, *Phys. Rev. B* **102**, 241115(R) (2020).
- [27] N. Astrakhantsev, F. Ferrari, N. Niggemann, T. Müller, A. Chauhan, A. Kshetrimayum, P. Ghosh, N. Regnault, R. Thomale, J. Reuther, T. Neupert, and Y. Iqbal, Pinwheel valence bond crystal ground state of the spin- $\frac{1}{2}$  Heisenberg antiferromagnet on the shuriken lattice, *Phys. Rev. B* **104**, L220408 (2021).
- [28] P. Schmoll, A. Kshetrimayum, J. Naumann, J. Eisert, and Y. Iqbal, Tensor network study of the spin- $\frac{1}{2}$  Heisenberg antiferromagnet on the shuriken lattice, *Phys. Rev. B* **107**, 064406 (2023).
- [29] J. Richter and J. Schnack, Magnetism of the  $s = \frac{1}{2}$   $J_1$ - $J_2$  square-kagome lattice antiferromagnet, *Phys. Rev. B* **107**, 245115 (2023).
- [30] M. Gembé, H.-J. Schmidt, C. Hickey, J. Richter, Y. Iqbal, and S. Trebst, Noncoplanar magnetic order in classical square-kagome antiferromagnets, *Phys. Rev. Research* **5**, 043204 (2023).
- [31] N. Niggemann, N. Astrakhantsev, A. Ralko, F. Ferrari, A. Maity, T. Müller, J. Richter, R. Thomale, T. Neupert, J. Reuther, Y. Iqbal, and H. O. Jeschke, Quantum paramagnetism in the decorated square-kagome antiferromagnet  $\text{Na}_6\text{Cu}_7\text{BiO}_4(\text{PO}_4)_4\text{Cl}_3$ , *Phys. Rev. B* **108**, L241117 (2023).
- [32] M. Fujihala, K. Morita, R. Mole, S. Mitsuda, T. Tohyama, S.-i. Yano, D. Yu, S. Sota, T. Kuwai, A. Koda, H. Okabe, H. Lee, S. Itoh, T. Hawaii, T. Masuda, H. Sagayama, A. Matsuo, K. Kindo, S. Ohira-Kawamura, and K. Nakajima, Gapless spin liquid in a square-kagome lattice antiferromagnet, *Nat. Commun.* **11**, 3429 (2020).
- [33] O. V. Yakubovich, L. V. Shvanskaya, G. V. Kiriukhina, A. S. Volkov, O. V. Dimitrova, and A. N. Vasiliev, Hydrothermal synthesis and a composite crystal structure of  $\text{Na}_6\text{Cu}_7\text{BiO}_4(\text{PO}_4)_4[\text{Cl},(\text{OH})]_3$  as a candidate for quantum spin liquid, *Inorganic Chemistry* **60**, 11450 (2021).
- [34] B. Liu, Z. Zeng, A. Xu, Y. Sun, O. Yakubovich, L. Shvanskaya, S. Li, and A. Vasiliev, Low-temperature specific-heat studies on two square-kagome antiferromagnets, *Phys. Rev. B* **105**, 155153 (2022).
- [35] M. Markina, P. Berdonosov, T. Vasilchikova, K. Zakharov, A. Murtazoev, V. Dolgikh, A. Moskvina, V. Glazkov, A. Smirnov, and A. Vasiliev, *Static and resonant properties of decorated square kagome lattice compound  $\text{KCu}_7(\text{TeO}_4)(\text{SO}_4)_5\text{Cl}$*  (2022), [arXiv:2212.11623](https://arxiv.org/abs/2212.11623) [cond-mat.str-el].
- [36] A. F. Murtazoev, K. A. Lyssenko, M. M. Markina, V. A. Dolgikh, A. N. Vasiliev, and P. S. Berdonosov, New Nabokoite-like Phases  $\text{ACu}_7\text{TeO}_4(\text{SO}_4)_5\text{Cl}$  ( $A = \text{Na}, \text{K}, \text{Rb}, \text{Cs}$ ) with Decorated and Distorted Square Kagome Lattices, *ChemPhysChem* **24**, e202300111 (2023).
- [37] O. Derzhko and J. Richter, Universal low-temperature behavior of frustrated quantum antiferromagnets in the vicinity of the saturation field, *Eur. Phys. J. B* **52**, 23 (2006).
- [38] X. Chen, S.-J. Ran, T. Liu, C. Peng, Y.-Z. Huang, and G. Su, Thermodynamics of spin-1/2 kagomé Heisenberg antiferromagnet: algebraic paramagnetic liquid and finite-temperature phase diagram, *Science Bulletin* **63**, 1545 (2018).
- [39] J. Schnack, J. Schulenburg, and J. Richter, Magnetism of the  $N = 42$  kagome lattice antiferromagnet, *Phys. Rev. B* **98**, 094423 (2018).
- [40] C. Hotta and K. Asano, Magnetic susceptibility of quan-

- tum spin systems calculated by sine square deformation: One-dimensional, square lattice, and kagome lattice Heisenberg antiferromagnets, *Phys. Rev. B* **98**, 140405 (2018).
- [41] J. Richter, O. Derzhko, and J. Schnack, Thermodynamics of the spin-half square kagome lattice antiferromagnet, *Phys. Rev. B* **105**, 144427 (2022).
- [42] J.-C. Domenge, P. Sindzingre, C. Lhuillier, and L. Pierre, Twelve sublattice ordered phase in the  $J_1 - J_2$  model on the kagomé lattice, *Phys. Rev. B* **72**, 024433 (2005).
- [43] O. Janson, J. Richter, and H. Rosner, Modified kagome physics in the natural spin-1/2 kagome lattice systems: Kapellasite  $\text{Cu}_3\text{Zn}(\text{OH})_6\text{Cl}_2$  and haydeelite  $\text{Cu}_3\text{Mg}(\text{OH})_6\text{Cl}_2$ , *Phys. Rev. Lett.* **101**, 106403 (2008).
- [44] L. Messio, C. Lhuillier, and G. Misguich, Lattice symmetries and regular magnetic orders in classical frustrated antiferromagnets, *Phys. Rev. B* **83**, 184401 (2011).
- [45] Y. Iqbal, H. O. Jeschke, J. Reuther, R. Valentí, I. I. Mazin, M. Greiter, and R. Thomale, Paramagnetism in the kagome compounds  $(\text{Zn}, \text{Mg}, \text{Cd})\text{Cu}_3(\text{OH})_6\text{Cl}_2$ , *Phys. Rev. B* **92**, 220404 (2015).
- [46] V. Grison, P. Viot, B. Bernu, and L. Messio, Emergent potts order in the kagome  $J_1 - J_3$  Heisenberg model, *Phys. Rev. B* **102**, 214424 (2020).
- [47] H.-J. Schmidt and J. Richter, Classical ground states of spin lattices, *J. Phys. A: Math. Theor.* **55**, 465005 (2022).
- [48] N. D. Mermin and H. Wagner, Absence of ferromagnetism or antiferromagnetism in one-or two-dimensional isotropic Heisenberg models, *Phys. Rev. Lett.* **17**, 1133 (1966).
- [49] S. Bieri, C. Lhuillier, and L. Messio, Projective symmetry group classification of chiral spin liquids, *Phys. Rev. B* **93**, 094437 (2016).
- [50] C. Hickey, L. Cincio, Z. Papić, and A. Paramekanti, Emergence of chiral spin liquids via quantum melting of noncoplanar magnetic orders, *Phys. Rev. B* **96**, 115115 (2017).
- [51] O. Janson, J. Richter, and H. Rosner, Intrinsic peculiarities of real material realizations of a spin-1/2 kagomé lattice, in *Journal of Physics: Conference Series*, Vol. 145 (IOP Publishing, 2009) p. 012008.
- [52] M. E. Zhitomirsky, Field-induced transitions in a kagomé antiferromagnet, *Phys. Rev. Lett.* **88**, 057204 (2002).
- [53] K. Hida, Magnetization process of the  $s=1$  and  $1/2$  uniform and distorted kagome Heisenberg antiferromagnets, *J. Phys. Soc. Jpn.* **70**, 3673 (2001).
- [54] J. Schulenburg, A. Honecker, J. Schnack, J. Richter, and H.-J. Schmidt, Macroscopic magnetization jumps due to independent magnons in frustrated quantum spin lattices, *Phys. Rev. Lett.* **88**, 167207 (2002).
- [55] A. Honecker, J. Schulenburg, and J. Richter, Magnetization plateaus in frustrated antiferromagnetic quantum spin models, *J. Phys.: Condens. Matter* **16**, S749 (2004).
- [56] H.-J. Schmidt, Theory of ground states for classical Heisenberg spin systems IV (2017), [arXiv:1710.00318](https://arxiv.org/abs/1710.00318).
- [57] D. Coffey and S. A. Trugman, Magnetic properties of undoped  $\text{C}_{60}$ , *Phys. Rev. Lett.* **69**, 176 (1992).
- [58] C. Schröder, H.-J. Schmidt, J. Schnack, and M. Luban, Metamagnetic phase transition of the antiferromagnetic Heisenberg icosahedron, *Phys. Rev. Lett.* **94**, 207203 (2005).
- [59] N. P. Konstantinidis, Antiferromagnetic Heisenberg model on clusters with icosahedral symmetry, *Phys. Rev. B* **72**, 064453 (2005).
- [60] N. P. Konstantinidis, Unconventional magnetic properties of the icosahedral symmetry antiferromagnetic Heisenberg model, *Phys. Rev. B* **76**, 104434 (2007).
- [61] N. Konstantinidis, Zero-temperature magnetic response of small fullerene molecules at the classical and full quantum limit, *J. Magn. Magn. Mater.* **449**, 55 (2018).
- [62] N. P. Konstantinidis,  $\Delta S^z=2$  quantum magnetization discontinuities proportional in number to the spin  $s$  in  $\text{C}_{60}$ : Origin and the role of symmetry, *SciPost Phys.* **15**, 037 (2023).
- [63] N. P. Konstantinidis, Origin of the classical magnetization discontinuities of the dodecahedron (2023), [arXiv:2311.17205](https://arxiv.org/abs/2311.17205) [cond-mat.str-el].
- [64] M. Zhitomirsky, M. Gvozdkova, and T. Ziman, Noncoplanar multi-k states in frustrated spinel and kagome magnets, *Ann. Phys.* **447**, 169066 (2022).
- [65] H.-J. Schmidt and J. Richter, Exotic magnetization curves in classical square-kagome spin lattices *J. Phys. A: Math. Theor.* **57**, 185001 (2024),.
- [66] R. Schmidt, J. Schnack, and J. Richter, Frustration effects in magnetic molecules, *J. Magn. Magn. Mater.* **295**, 164 (2005).
- [67] J. Schnack and R. Schnalle, Frustration effects in antiferromagnetic molecules: the cuboctahedron, *Polyhedron* **28**, 1620 (2009).
- [68] H.-J. Schmidt and M. Luban, Classical ground states of symmetrical Heisenberg spin systems, *J. Phys. A: Math. Gen.* **36**, 6351 (2003).
- [69] C. Lanczos An iteration method for the solution of the eigenvalue problem of linear differential and integral operators, *J. Res. Nat. Bur. Stand.* **45**, 255-282 (1950).
- [70] J. Jaklič and P. Prelovšek, Lanczos method for the calculation of finite-temperature quantities in correlated systems, *Phys. Rev. B* **49**, 5065-5068 (1994)